Plasma-Enhanced CVD Synthesis and Structural Characterization of Ta_2N_3

Alexei Yu. Ganin,[a] Lorenz Kienle,[a] and Grigori V. Vajenine*[a,b]

Dedicated to Professor Francis J. DiSalvo on the occasion of his 60th birthday

Keywords: Tantalum / Nitrides / Plasma-enhanced chemical vapor deposition / X-ray diffraction / Electron microscopy

Microcrystalline tantalum nitride films were prepared on various substrates from $TaCl_5$ precursor and nitrogen gas using the plasma-enhanced chemical vapor deposition (PECVD) method. Syntheses carried out at 600–650 °C led to single-phase samples of the tantalum nitride Ta_2N_3 with a defect fluorite-type structure. The anion vacancies were found to order resulting in a $2 \times 2 \times 2$ cubic superstructure of the C-Ln_2O_3 type (space group $Ia\bar{3}$, $Z = 16$) with a = 9.8205(4) Å according to a Rietveld refinement of the X-ray powder diffraction data. At higher deposition temperatures (650–700 °C) formation of highly textured orthorhombic Ta_3N_5 was observed. The samples were additionally studied by high-resolution transmission electron microscopy (HRTEM) and selected-area electron diffraction (SAED). The details of the new crystal structure for Ta_2N_3 as well as a possible nitrogen nonstoichiometry are discussed.

Introduction

The binary Ta−N system is quite rich in compounds with well-defined and variable stoichiometries. The formal oxidation state of tantalum covers the whole range from nearly zero to the maximum of +5. These compounds can be divided into four groups: solid solutions of nitrogen in tantalum, the phase with the approximate stoichiometry Ta_2N, three phases with a nearly 1:1 composition, and nitrogen-rich nitrides. A few comprehensive reviews of tantalum nitride structural chemistry are available.[1−3] Results of the previous structural studies in this binary system are summarized in Table 1.

Up to 5 at.% of nitrogen can be dissolved in the body-centered cubic lattice of elemental tantalum, for example by heating of Ta powder in ammonia at 600−700 °C.[3] The lattice constant of such solid solutions increases slightly to 3.315−3.369 Å compared to that of the pure metal (a = 3.311 Å). Observation of additional weak reflections suggests a cubic superstructure with the unit cell tripled in all directions and with $a_\beta = 3a_\alpha = 10.11$ Å.[1,13]

The γ-phase with the composition range $TaN_{0.41-0.5}$, also denoted as β-Ta_2N,[4] crystallizes with a hexagonal unit cell.[1−4] Its crystal structure can be described as a hexagonal close packing of the tantalum atoms with the nitrogen atoms filling half of the octahedral interstices. While the earlier studies suggested a statistical distribution,[1,2] electron-[3] and neutron-diffraction[4] investigations revealed a trigonal $P\bar{3}1m$ supercell with $a' = \sqrt{3}a$, isostructural to β-Nb_2N[14] and of the anti-Li_2ZrF_6-type.[15] The γ-phase can be obtained by nitriding of tantalum powder in gaseous ammonia at 800−900 °C or from the elements at 2000 °C.[1,3]

The hexagonal ε-phase was proposed by Schoenberg[1] to have a B35 CoSn-type structure with the composition $TaN_{1.00}$; the same description was given by Brauer and Zapp.[2] In this structure type the nitrogen atoms are at the center of slightly distorted tantalum octahedra. Later, Christensen and Lebech[5] showed that the nitrogen atoms are displaced from these ideal positions reducing their coordination sphere to a square pyramid. The unit cell determined by Christensen and Lebech[5] (a = 5.196 Å, c = 2.911 Å) is quite similar to that given by the other authors.[1−3] The ε-phase can be obtained as a product of nitriding of Ta powder at temperatures at > 1100 °C.[1]

Another modification of tantalum mononitride, the δ-phase with a face-centered cubic B1 NaCl-type structure, was observed by Gerstenberg and Calbick[16] in thin films; it was also recently synthesized from the ε-phase by shock compression.[7] The lattice parameter (a = 4.337 Å) for this

[a] Max-Planck-Institut für Festkörperforschung
Heisenbergstraße 1, 70569 Stuttgart, Germany
Fax: (internat.) + 49-711-689-1091
E-mail: G.Vajenine@fkf.mpg.de
A.Ganine@fkf.mpg.de
L.Kienle@fkf.mpg.de
[b] Institut für Anorganische Chemie, Universität Stuttgart,
Pfaffenwaldring 55, 70569 Stuttgart, Germany
Supporting information for this article is available on the WWW under http://www.eurjoc.org or from the author.

Table 1. Structural overview of known tantalum nitrides

Phase	Crystal structure	Composition	Lattice parameters [Å] a	c	Ref.
α-phase	body-centered cubic, A2 W-type	Ta	3.311		[1]
		$TaN_{0.04}$	3.315		[2]
β-phase	α-phase with a cubic 3 × 3 × 3 superstructure	$TaN_{0.05}$	10.11 (3× 3.369)		[1]
γ-phase (β-Ta_2N)	hexagonal close-packing of the tantalum atoms	$TaN_{0.41}$	3.041	4.907	[1]
		$TaN_{0.5}$	3.042	4.905	[2]
	an anti-Li_2ZrF_6-type superstructure with $a' = \sqrt{3}a$	$TaN_{0.5}$	5.283 ($\sqrt{3}$ × 3.050)	4.928	[3]
		$TaN_{0.43}$	5.285 ($\sqrt{3}$ × 3.051)	4.919	[4]
ε-phase	hexagonal, B35 CoSn-type	$TaN_{1.00}$	5.185	2.908	[1]
		$TaN_{1.00}$	5.181	2.905	[2]
		$TaN_{1.00}$	5.188	2.903	[3]
	hexagonal, distorted B35 CoSn-type	$TaN_{1.00}$	5.196	2.911	[5]
δ-phase	face-centered cubic, B1 NaCl-type	$TaN_{0.92}$	4.337		[6]
		$TaN_{0.97}$	4.336		[7]
θ-phase	hexagonal, Bh WC-type	$TaN_{1.00}$	2.936	2.885	[8]
		$TaN_{1.08}$	2.938	2.868	[9]
Ta_3N_5	orthorhombic, Fe_2TiO_5-type	Ta_3N_5	3.8862	b = 10.2118 c = 10.2624	[10]
Ta_4N_5	tetragonal, Nb_4N_5-type	Ta_4N_5	6.835	4.272	[3]
Ta_5N_6	hexagonal, Nb_5N_6-type	Ta_5N_6	5.175	10.307	[3]
TaN_x	cubic, CaF_2-type	TaN_x	5.02		[11]
	CaF_2-type with a body-centered tetragonal superstructure	TaN_x	5.77	5.01	[12]

nitride obtained by Gatterer et al.[6] from the elements at 2000 °C and a pressure of 40 bar, and that obtained by Mashimo et al.[7] (a = 4.336 Å), are almost identical.

Finally, the θ-phase crystallizes hexagonal in the Bh WC-type structure type with a simple hexagonal stacking of the metal layers. The nitrogen atoms center the trigonal prisms formed by the tantalum atoms. The unit cell observed for this hexagonal phase (a = 2.936 Å, c = 2.885 Å) by Brauer et al.[8] is rather similar to that obtained by Mashimo and Tashiro[9] (a = 2.938 Å, c = 2.868 Å). The hexagonal ε-TaN phase transforms into θ-TaN at pressures of 20−100 kbar and at 800−960 °C, or under mechanical alloying conditions.[8,9]

Ta_3N_5, the nitrogen-richest phase, has a pseudobrookite (Fe_2TiO_5)-type[17] structure. This structure contains octahedrally coordinated tantalum atoms, while the nitrogen atoms are both three- and four-coordinate. The TaN_6 octahedra are linked together by sharing edges and corners. Though Brauer and Weidlein[18] reported a tetragonal unit cell, it was later refined as orthorhombic[19] (a = 3.893 Å, b = 10.264 Å, c = 10.264 Å) and monoclinic[20] (a = 10.229 Å, b = 3.875 Å, c = 10.229 Å, β = 90.0°). Brese et al.[10] have shown that both structural models are valid within the accuracy of the data. Ta_3N_5 can be obtained by nitriding of Ta_2O_5 in an ammonia flow at 860−920 °C,[18] for example.

Upon heating in argon or ammonia, Ta_3N_5 decomposes yielding the nitrides Ta_4N_5 and Ta_5N_6.[21] The tetragonal Ta_4N_5[3] phase is isostructural to Nb_4N_5,[22] a defect variant of the NaCl-type structure. The hexagonal Ta_5N_6[3] is isostructural to Nb_5N_6;[22] it is built up from the tantalum atom layers in the stacking ABACABAC.

Yet another binary tantalum nitride, TaN_x, has been reported, although its stoichiometry and crystal structure have not been established reliably. It was first observed in reactive sputtering experiments by Buvinger[11] and appeared to have an fcc-type crystal structure with a = 5.02 Å, which is notably larger than that of the NaCl-type δ-phase (a = 4.34 Å). Coyne and Tauber[12] confirmed the lattice parameter range of 4.98−5.05 Å and proposed a fluorite-type structure for this nitride. Additional reflections led the authors to postulate a body-centered tetragonal supercell with a = 5.77 Å and c = 5.01 Å.

Except for the latter phase, all the above-mentioned tantalum nitrides can be prepared by conventional synthetic routes. In the last few years interest in tantalum nitride films has been sparked by a combination of their mechanical stability, chemical inertness and resistive behavior of these phases. Possible applications in microelectronics as Cu diffusion barriers, for example, has stimulated application of novel techniques such as reactive sputtering,[23,24] rapid thermal processing,[25] and ion-beam-assisted deposition (IBAD)[26] to the synthesis of tantalum nitrides. Another approach, the plasma-enhanced chemical vapor deposition (PECVD) method proved to be useful for the preparation of the cubic δ-phase, for example.[27,28] This contribution describes the application of PECVD to the synthesis of Ta_2N_3, previously known as the "bct-TaN_x" phase, and its structural characterization.

Results and Discussion

Tantalum nitride powder coatings were grown in a PECVD reactor by passing a mixture of nitrogen gas and $TaCl_5$ precursor in the plasma region over the substrate in the temperature range of 600−700 °C. Deposition experiments were carried out on silicon, copper, and quartz glass

Table 2. PECVD conditions, product composition, and unit cell parameters for selected samples

Sample	Phase composition	N/Ta ratio from EDXS	$a(Ta_2N_3)$ [Å]	Deposition temp. [°C]	Substrate
A	Ta_2N_3	1.35(4)	9.841(4)	630	Si (100)
B	Ta_3N_5	1.48(3)	–	715	Si (100)
C	Ta_2N_3	1.41(3)	9.8205(4)	640	Si (100)
D	Ta_2N_3	1.35(4)	9.822(6)	640	Si (100)
E	Ta_2N_3	1.36(4)	9.850(5)	635	Si (100)
F	Ta_2N_3	1.42(4)	9.862(4)	640	Cu
G	Ta_2N_3	1.28(4)	9.844(4)	620	Cu
H	Ta_2N_3	1.26(4)	9.803(3)	625	quartz glass
I	Ta_2N_3 + Ta_3N_5	1.45(3)	9.863(5)	670	Si (100)
J	Ta_3N_5 + TaN	1.33(4)	–	–	–

substrates. Representative deposition conditions are listed in Table 2.

The phase composition of the coatings varies with the deposition temperature, according to the powder X-ray diffraction investigations. While at higher temperatures of 650−700 °C the orthorhombic Ta_3N_5 phase was predominantly formed, the experiments at lower temperature (600−650 °C) yielded another phase with the strongest reflections corresponding to an fcc lattice with $a \approx 5.0$ Å. This value, which is similar to that observed for the "bct-TaN_x" phase, suggested a nitrogen-rich phase of the fluorite (CaF_2) type. However, the ideal composition "TaN_2" is implausible due to the requirement of the formal oxidation state Ta^{6+}. Indeed, a closer inspection of the additional weak reflections indicated a cubic $2 \times 2 \times 2$ superstructure. The analogy to the well-known bixbyite- or C-Ln_2O_3-type phases[29,30] (space group $Ia\bar{3}$) led us to postulate the same structure and the Ta_2N_3 composition for this tantalum nitride. It was mentioned above that a similar fluorite-based TaN_x phase has been identified by electron diffraction in samples obtained in sputtering experiments.[12] Weak superstructure reflections were observed there as well, but a different body-centered tetragonal supercell with $a = 5.77$ Å and $c = 5.01$ Å was proposed without further structural study.[12] However, these superstructure reflections appear to be identical to those observed in our study; moreover, the c/a ratio of the proposed bct cell is $0.867 \approx \sqrt{3}/2$, indicating the equivalence of the $(200)_{bct}$ and $(111)_{fluorite}$ reflections according to the cell choices of the phases. This would imply non-orthogonality of the proposed a_{bct} and c_{bct} axes, thus making the bct superstructure inadequate.

The product composition was determined by energy-dispersive X-ray spectroscopy (EDXS). Although the formation of nitrogen-rich products could be established, more accurate determination of the composition was not possible. Chlorine contamination was found to be below the detection limit of EDXS (2−3 at.%), whereas the oxygen content did not exceed 5 at.%.

In order to test the proposed structural model for Ta_2N_3, sample A was investigated by HRTEM and was additionally studied with the internal EDX. As before, only a small amount of oxygen (less then 4 at.%) was found in the sample; no other impurities could be detected. Such oxygen content typically results from the surface contamination of thin crystallites. Sample A contains irregular, roundish particles with sizes in the range of 50−500 nm (Figure 1a). Electron-diffraction patterns recorded on aggregates of particles show Bragg intensities located on concentric rings around 000. The d values derived from these patterns are consistent with the metrics of the cubic Ta_2N_3 phase. Applying selected-area electron diffraction (SAED), the larger roundish particles of the sample could be identified as microcrystals of Ta_2N_3. SAED patterns were recorded along different zone axes on these crystallites in order to compare them with simulated patterns. Some crystallites of sample A were sufficiently large and could be tilted in several zone axis orientations. The tilt angles, α, are consistent with the expected cubic metrics, for example with those for the zone axes $[100]_{cubic}$ and $[311]_{cubic}$ ($\alpha = 25.2°$), $[311]_{cubic}$ and $[211]_{cubic}$ ($\alpha = 10°$), and $[111]_{cubic}$ and $[313]_{cubic}$ ($\alpha = 22°$). For all analyzed orientations, we observed a convincing agreement between the simulated and experimental patterns (see Figure 1b for $[100]_{cubic}$).

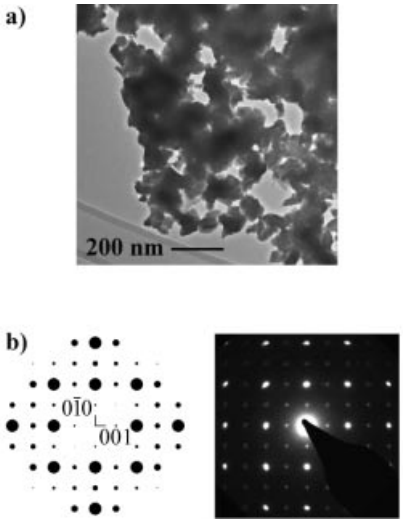

Figure 1. High resolution transmission electron microscopy (HRTEM) micrographs of deposited tantalum nitride: (a) roundish shape of Ta_2N_3 crystallites; (b) simulated and observed selected-area electron diffraction patterns along the [100] axis

Through-focus HRTEM images, for instance in [110] orientations, are in good agreement with simulated micrographs based on the assumed structure of Ta_2N_3. However, details of the real structure concerning the precise arrangement of the nitrogen atoms cannot be derived from HRTEM micrographs.

The C-Ln_2O_3 structure type is an ordered-defect variant of the fluorite structure. Aside from doubling of the unit cell in all directions, a quarter of the anion positions remain empty. When local coordination of the Ta atoms is considered, this corresponds to removing two of eight nitrogen atoms in the first coordination sphere on going from the ideal TaN_2 composition to the stoichiometry Ta_2N_3. Two types of Ta positions result, as shown in Figure 2a: while two opposing nitrogen atoms of a TaN_8 cube are removed around Ta(1), two nitrogen positions connected by a face diagonal of the cube remain empty for Ta(2). After a relaxation of the crystal structure, Ta(1) occupies the 8*b* position (1/4,1/4,1/4), Ta(2) is shifted to the 24*d* site (*x*,0,1/4), and the nitrogen atoms take the general 48*e* position with $x \approx z \approx 3/8$ and $y \approx 1/8$ (see Table 3). The missing nitrogen atoms would occupy the 16*c* (*x*,*x*,*x*) site with $x \approx 1/8$ in this space group. Partial filling of the latter position is indeed observed in the $U_2N_{3+\delta}$ series, in which both end members, U_2N_3 and UN_2, are known as well.[31]

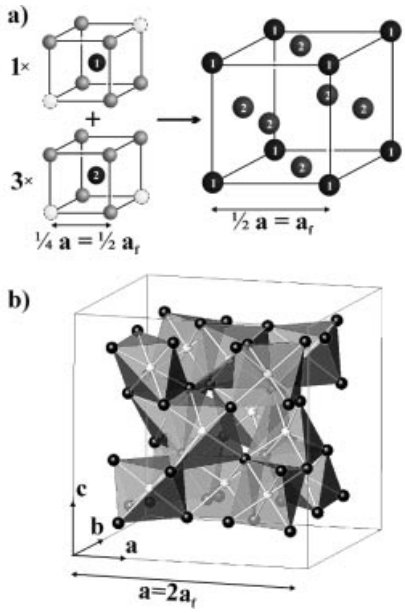

Figure 2. Crystal structure of Ta_2N_3: (a) analogy between the fluorite and Ta_2N_3 structures ["1" and "2" stand for the Ta(1) and Ta(2) positions, respectively]; (b) TaN_6 coordination polyhedra inside the unit cell of Ta_2N_3

While the TEM and SAED investigations confirmed qualitatively the C-Ln_2O_3-type structure for this tantalum nitride, a Rietveld refinement of the powder diffraction data from sample C was carried out in order to elucidate the structural details. It was possible to refine the atomic positions for all atoms; these are shown in Table 3, in comparison with those in related phases.

Table 3. Atomic positions in Ta_2N_3 compared to those in related compounds

	x(24*d*)	*x*(48*e*)	*y*(48*e*)	*z*(48*e*)
Ta_2N_3	−0.0280(3)	0.377(4)	0.153(3)	0.377(6)
Ta_2N_3 model	−0.02686	0.38366	0.14472	0.38061
U_2N_3 [31]	−0.018	0.38	0.167	0.398
Y_2O_3 [32]	−0.0320(1)	0.3911(5)	0.1516(5)	0.3827(6)
Zn_3N_2 [33]	−0.0216(1)	0.3975(1)	0.1498(2)	0.3759(1)
Mg_3N_2 [34]	−0.031(2)	0.38925(6)	0.15217(7)	0.38220(6)
Ca_3N_2 [34]	−0.03826(18)	0.39006(3)	0.15389(3)	0.38242(3)
Ideal fluorite	0	3/8	1/8	3/8

The refinement of the occupation of the 16*c* position was not successful due to the low quality of the powder diffraction data; this position was left empty in the further refinements. The resulting crystal structure of Ta_2N_3 is shown in Figure 2. The structure is built from octants, which have tantalum atoms in their centers. These form a face-centered cubic lattice and are coordinated by distorted octahedra of nitrogen atoms. The TaN_6 units are linked together by sharing edges and corners. The Ta−N distances in two different Ta coordination polyhedron types vary between 2.01(5) and 2.17(4) Å. Similar Ta−N distances were found in the nitrides Ta_3N_5 (1.955−2.240 Å), ε-TaN (2.041−2.163 Å), δ-TaN (2.165 Å), and θ-TaN (2.23 Å). In the Ta(1)N_6 trigonal antiprisms all Ta(1)−N distances are equal to 2.01(5) Å and the bond angles [78(2)−108(2) and 180°] approach those in an ideal octahedron. The Ta(2)N_6 polyhedron is less symmetrical: there are three pairs of Ta(2)−N distances [2 × 2.13(4), 2 × 2.13(5), and 2 × 2.17(4) Å] and the bond angles fall into the ranges 72(2)−116(2) and 129(2)−170(2)°. The coordination of nitrogen atoms remains nearly tetrahedral, as in the parent fluorite structure, with the Ta−N−Ta bond angles ranging from 100(2) to 125(2)°.

Due to a relatively large uncertainty in the nitrogen position, a simple model structure was introduced. First, for each value of $x_{Ta(2)}$, a nitrogen position equidistant from the four tantalum neighbors was calculated. The resulting Ta−N distance was then plotted as a function of $x_{Ta(2)}$ (Figure 3). Remarkably, this function was found to reach a minimum at $x_{Ta(2)} = -0.02686$ with a corresponding Ta−N distance of 2.109 Å. The resulting model structure may be taken as the first approximation to a crystal structure involving chemically similar Ta(1) and Ta(2) atoms. As Table 3 shows, this model reproduces well the observed Ta_2N_3 structure: the corresponding structural parameters compare well with the refined ones, when the respective standard deviations are taken into account.

The question of the exact stoichiometry of Ta_2N_3 remains open: a partial occupation of the 16*c* position, as in $U_2N_{3+\delta}$, leading to $Ta_2N_{3+\delta}$ cannot be excluded. Since the highest formal oxidation state of tantalum is +5, the values of δ from 0 to 1/3 are possible. The EDXS method is not sensitive enough to detect such a small variation of the composition and sufficiently large amounts of Ta_2N_3 for an accurate chemical analysis cannot yet be prepared. Larger

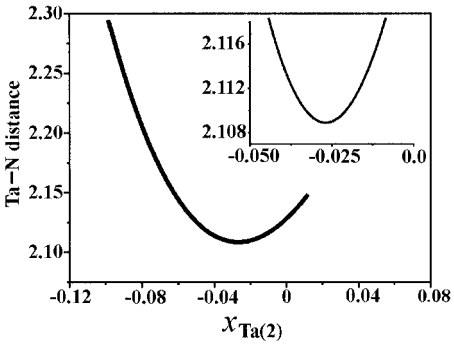

Figure 3. The Ta−N bond length in a Ta_2N_3 model structure in Å as a function of the Ta(2) *x*-coordinate assuming the equality of all Ta−N distances

samples would also be required for accurate measurements of resistivity and magnetic susceptibility. Interestingly, the "bct-TaN_x" phase[12] was found to be conducting, with a ρ(T) behavior corresponding to $\Delta E \approx 0.1-0.3$ eV and with an optical bandgap of 2.0−2.6 eV. Two indirect indications suggest that the formal oxidation state of tantalum in $Ta_2N_{3+\delta}$ is lower than +5. Firstly, the color of the compound (black metallic) compared to that of Ta_3N_5 (red-brown) supports this idea. Secondly, annealing $Ta_2N_{3+\delta}$ samples in vacuo at 700 °C led to an apparent disproportionation to fcc δ-TaN and Ta_3N_5 (see also Table 2), thus also suggesting a lower tantalum oxidation state. Therefore, we designate this phase as Ta_2N_3, keeping the possible nitrogen nonstoichiometry in mind.

In sample B, which contains Ta_3N_5 with a small fraction of Ta_2N_3, nanorods (see Figure 4a) with typical dimensions

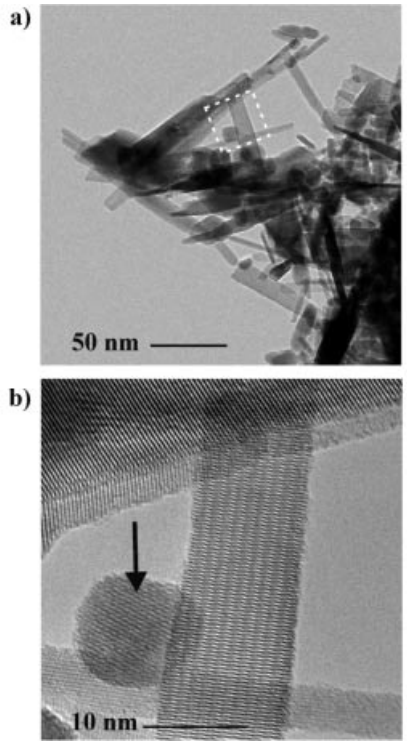

Figure 4. (a) Nanorods of Ta_3N_5; (b) enlarged section: a crystallite of Ta_2N_3 (see arrow) bordered by the Ta_3N_5 nanorods

of 10 nm × 100 nm were observed by HRTEM. In the diffraction patterns of these nanorods strong intensities occur in the positions expected for the orthorhombic Ta_3N_5 phase. All nanorods are highly crystalline (Figure 4b). These microcrystals of Ta_3N_5 exhibit additional features of the micro- and nanostructure which both originate from a lamellar assembly of $(010)_{ortho}$ layers.

Conclusion

Microcrystalline films of a binary tantalum nitride with the composition Ta_2N_3 have been obtained in an RF plasma from $TaCl_5$ and nitrogen gas at 600−650 °C using the PECVD technique. According to X-ray and electron diffraction data, the compound crystallizes in the cubic C-Ln_2O_3 structure type, an ordered defect 2 × 2 × 2 superstructure of the fluorite type. This nitride is thought to be identical with the previously reported "bct-TaN_x" phase obtained in sputtering experiments. Notably, this binary tantalum nitride could not be prepared by conventional synthetic routes so far; plasma activation of the nitrogen gas appears to be essential for the successful synthesis.

Experimental Section

Synthesis: Syntheses were performed in a custom-designed PECVD (Plasma Enhanced Chemical Vapor Deposition) experimental setup, which is schematically illustrated in Figure 5. It consists of a nitrogen gas delivery line, a precursor handling system, and a reactor.

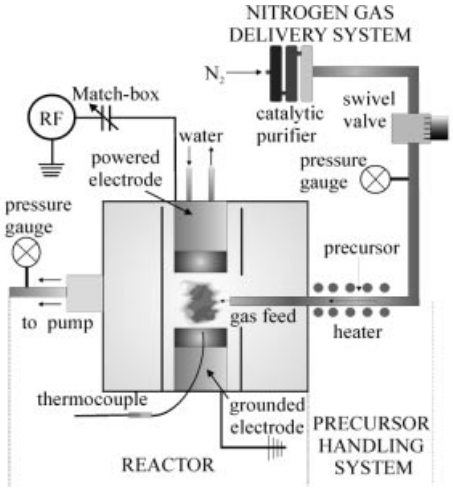

Figure 5. Scheme of the experimental PECVD setup

Nitrogen Gas Delivery Line: Nitrogen gas (Westfalen AG, 99.999%) was further purified by passing it through three separate catalytic columns (silica gel, molecular sieves, and an oxysorb catalyst[35]), in order to remove traces of oxygen and moisture from the nitrogen stream.

Precursor Handling System: The $TaCl_5$ precursor was loaded in a argon dry box into a glass tube, which was then connected to the setup under nitrogen flow. The precursor was then dropped down into the heated delivery line. Throughout the deposition process the temperature of the precursor handling system was maintained at 70−80 °C by means of a hot air gun in order to prevent the condensation of the precursor.

Reactor: Deposition occurred in a plasma region inside of a quartz tube between two parallel electrodes. This setup was placed in an evacuated glass vessel. The upper of the electrodes was connected to the 13.56 MHz 1000 W RF (radio frequency) source (Hüttinger, PFG-RF1000) through a match box (Hüttinger, PFM 1500A), while the lower electrode was grounded. Substrates were loaded on the lower electrode, the upper electrode was water-cooled. An NiCr/NiAl thermocouple was inserted into the lower electrode for temperature monitoring as shown in Figure 5.

Deposition: Before every deposition, the reactor with a loaded substrate was baked in plasma at 400 °C in the nitrogen gas flow for 1 h. Afterwards, the reactor was cooled and heated up to the deposition temperature by igniting the plasma. Nitrogen carrier gas was mixed with the $TaCl_5$ precursor evaporated at 70−80 °C and delivered into the gap between the two electrodes. The pressure in the system was measured by means of two pressure gauges at the inlet and the outlet of the setup. The deposition time varied depending on the evaporation rate of the $TaCl_5$ precursor. A typical experiment took 2−6 h at an RF power of 500−700 W. The reaction progress could also be monitored by the color change of the plasma from light green to yellow-orange as the precursor was consumed. The conditions of the deposition experiments are summarized in Table 2.

Substrates: Silicon wafer (100), copper (Alfa Aesar, 99.9%), and quartz glass substrates (Heraeus) were used. Their sizes varied from 5 × 10 to 10 × 20 mm. The substrates were prepared for deposition by washing with ethanol in a sonic bath and then rinsing with deionized water and acetone.

Precursor Preparation: Tantalum(v) chloride (Alfa Aesar, 99.99% metals basis) was purified by sublimation. The observed X-ray diffraction pattern of the product matched that of the monoclinic phase reported in the literature.[36]

Scanning Electron Microscopy Analysis: Investigations were performed with a TESCAN 5120MM scanning electron microscope. Quantitative analysis of the samples was done by EDXS with an Oxford Si-detector with an electron-beam energy of 10 keV, and signal accumulation time of 60−120 s.

Transmission Electron Microscopy: Samples A (Ta_2N_3) and B (Ta_3N_5) were crushed in an agate mortar and suspended in *n*-butanol. A perforated carbon/copper net was covered with the suspension, leaving wedge-shaped crystallites in random orientations after drying. HRTEM and SAED investigations were performed with a Philips CM30ST instrument (300 kV, LaB_6 cathode, C_S = 1.15 mm). Computer simulations of the HRTEM images (multislice formalism) and SAED patterns (kinematical approximation) were carried out with the EMS program package[37] (spread of defocus: 70 Å, illumination semiangle: 1.2 mrad). All images were collected with a Multiscan CCD Camera [software Digital Micrograph 3.6.1 (Gatan)].

Sample Appearance: The deposits of Ta_2N_3 were black with a metallic shine; growth of red-brown Ta_3N_5 was also observed in some experiments. Adhesion of all samples to the substrate material was rather low, as evidenced by the "scotch test": the microcrystalline products could be removed from the substrates by a scotch tape.

Annealing: Sample I (Ta_2N_3) was annealed at 700 °C in vacuo (5.0×10^{-8} Torr) for 50 h. X-ray analysis of the sample was carried out before and after the annealing.

X-ray Crystallographic Study: The powder diffraction data were collected with a STADI-P STOE diffractometer using Cu-$K_{\alpha 1}$ radiation at room temperature. The results of the phase analysis are presented in Table 2. The powder diffraction pattern of the single phase sample C is shown in Figure 6, where the reflections corresponding to the 2 × 2 × 2 superstructure of the fluorite unit cell are clearly visible. These data were used for a Rietveld refinement using the CSD package.[38] The C-Ln_2O_3 structure type (space group $Ia\bar{3}$) was chosen as the starting model for Ta_2N_3. The unit cell constant and the atomic positional parameters were refined, while the isotropic temperature displacement factor had to be fixed for the nitrogen atom position; pseudo-Voigt functions were employed to model the reflection profiles. The background was fitted by a parabolic form, and an absorption correction was introduced. Additionally, texture effects along the [100] axis had to be taken into account. Crystal data for the investigated sample are summarized in Table 4. Further details of the crystal structure investigation may be obtained from the Fachinformationzentrum Karlsruhe, 76344 Eggenstein-Leopoldshafen, Germany, on quoting the depository number CSD-413802.

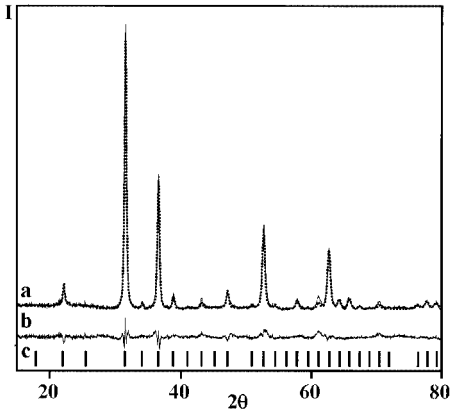

Figure 6. (a) Measured powder X-ray diffraction pattern of Ta_2N_3 (solid line) and the calculated curve (dotted line); (b) the difference curve; (c) positions of the Ta_2N_3 reflections

Table 4. Details of the crystal structure refinement for Ta_2N_3

Radiation, wavelength	Cu-$K_{\alpha 1}$, 1.54051 Å
Crystal system, space group	cubic, $Ia\bar{3}$ (no. 206), Z = 16
Unit cell dimensions [Å]	a = 9.8205(4)
Unit cell volume [Å^3]	947.1(1)
Refinement method	full profile
2θ range [°]	15−80
Free parameters	10
Final R values	R(intensity) = 8.75%; R(profile) = 18.06%

Acknowledgments

This work was supported by the Sofja Kovalevskaja Research Award of the Alexander von Humboldt Foundation, the Federal Ministry of Education and Research, and Programme for Investment in the Future (ZIP) of the German Government. We also thank Professor Arndt Simon for his support, Mitsuharu Konuma for valuable advice on the PECVD setup, and Viola Duppel and Claudia Kamella for EDX and HRTEM measurements.

[1] N. Schönberg, *Acta Chem. Scand.* **1954**, *8*, 199−203.
[2] G. Brauer, K. H. Zapp, *Z. Anorg. Allg. Chem.* **1954**, *277*, 129−139.
[3] N. Terao, *Jpn. J. Appl. Phys.* **1971**, *10*, 249−259.
[4] L. E. Conroy, A. N. Christensen, *J. Solid State Chem.* **1977**, *20*, 205−207.
[5] A. N. Christensen, B. Lebech, *Acta Crystallogr., Sect. B* **1978**, *34*, 261−263.
[6] J. Gatterer, G. Dufek, P. Ettmayer, R. Kieffer, *Monatsh. Chem.* **1975**, *106*, 1137−1147.
[7] T. Mashimo, S. Tashiro, T. Toya, H. Yamazaki, S. Yamaya, K. Oh-ishi, Y. Syono, *J. Mater. Sci.* **1993**, *28*, 3439−3443.
[8] G. Brauer, E. Mohr, A. Neuhaus, A. Skogan, *Monatsh. Chem.* **1972**, *103*, 794−798.
[9] T. Mashimo, S. Tashiro, *J. Mater. Sci. Lett.* **1994**, *13*, 174−176.
[10] N. E. Brese, M. O'Keeffe, P. Rauch, F. J. DiSalvo, *Acta Crystallogr., Sect. C* **1991**, *47*, 2229−2294.
[11] E. A. Buvinger, *Appl. Phys. Lett.* **1965**, *7*, 14−15.
[12] H. J. Coyne, R. N. Tauber, *J. Appl. Phys.* **1968**, *39*, 5585−5593.
[13] D. P. Seraphim, N. R. Stemple, D. T. Novick, *J. Appl. Phys.* **1962**, *33*, 136−141.
[14] A. N. Christensen, *Acta Chem. Scand., Ser. A* **1976**, *30*, 219−224.
[15] R. Hoppe, W. Daehne, *Naturwissenschaften* **1960**, *47*, 397.
[16] D. Gerstenberg, C. J. Calbick, *J. Appl. Phys.* **1964**, *35*, 402−407.
[17] L. Pauling, *Z. Kristallogr., Kristallgeom., Kristallphys., Kristallchem.* **1930**, *73*, 97−113.
[18] G. Brauer, J. R. Weidlein, *Angew. Chem.* **1965**, *77*, 218−219; *Angew. Chem. Int. Ed. Engl.* **1965**, *4*, 241.
[19] J. Straehle, *Z. Anorg. Allg. Chem.* **1973**, *402*, 47−57.
[20] N. Terao, *C. R. Acad. Sci. Ser. C* **1977**, *285*, 12−20.
[21] J-C. Gilles, *C. R. Acad. Sci. Ser. C* **1968**, *266*, 546−547.
[22] N. Terao, *J. Less-Common Met.* **1971**, *23*, 159−169.
[23] T. Riekkinen, J. Molarius, T. Laurilab, A. Nurmela, I. Suni, J. K. Kivilahti, *Microelectron. Eng.* **2002**, *64*, 289−297.
[24] C. S. Shin, Y. W. Kim, D. Gall, J. E. Greene, I. Petrov, *Thin Solid Films* **2002**, *402*, 172−182.
[25] C. Angelkorta, A. Berendes, H. Lewaltera, W. Bock, B. O. Kolbesen, *Thin Solid Films* **2003**, *437*, 108−115.
[26] K. Volz, M. Kiuchi, W. Ensinger, *Surf. Coat. Technol.* **2000**, *128*, 298−302.
[27] X. Chen, H. L. Frisch, A. E. Kaloyeros, *J. Vac. Sci. Technol. B* **1999**, *17*, 182−185.
[28] X. Chen, G. G. Peterson, C. Goldberg, G. Nuesca, H. L. Frisch, A. E. Kaloyeros, B. Arkles, J. Sullivan, *J. Mater. Res.* **1999**, *14*, 2043−2052.
[29] F. S. Galasso, *Structure and Properties of Inorganic Solids*, 1st ed., Pergamon Press, Oxford, **1970**, p. 99.
[30] A. F. Wells, *Structural Inorganic Chemistry*, 4th ed., Clarendon Press, Oxford, **1975**, p. 451.
[31] R. E. Rundle, N. C. Baenzinger, A. S. Wilson, R. A. McDonald, *J. Am. Chem. Soc.* **1948**, *70*, 99−105.
[32] L. Smrcok, *Cryst. Res. Technol.* **1989**, *24*, 607−611.
[33] D. E. Partin, D. J. Williams, M. O'Keefe, *J. Solid State Chem.* **1997**, *132*, 56−59.
[34] O. Reckeweg, F. J. DiSalvo, *Z. Anorg. Allg. Chem.* **2001**, *687*, 371−377.
[35] B. Horvath, J. Strutz, J. Geyer-Lippmann, E. G. Horvath, *Z. Anorg. Allg. Chem.* **1981**, *209*, 483.
[36] S. Rabe, U. Müller, *Z. Kristallogr. − New Cryst. Struct.* **2000**, *215*, 1−2.
[37] P. A. Stadelmann, *Ultramicroscopy* **1987**, *21*, 131.
[38] L. G. Akselrud, Yu. N. Grin, P. Yu. Zavalij, V. K. Percharsky, V. S. Fundamenskii, "CSD − Universal program package for single crystal and/or powder structure data treatment", *12th European crystallographic meeting: Abstract of papers*, Moscow, **1989**, vol. 3, p. 155.

Received March 22, 2004
Early View Article
Published Online July 12, 2004

